Physical-model-based reconstruction of axisymmetric three-dimensional sound field from optical interferometric measurement

OPEN ACCESS
IOP Publishing
Measurement Science and Technology
Meas. Sci. Technol. **32** (2021) 045202 (8pp)
https://doi.org/10.1088/1361-6501/abce73

Physical-model-based reconstruction of axisymmetric three-dimensional sound field from optical interferometric measurement

Kenji Ishikawa[1,2], **Kohei Yatabe**[1] **and Yasuhiro Oikawa**[1]

[1] Department of Intermedia Art and Science, Waseda University, 3-4-1 Ohkubo, Shinjuku-ku, Tokyo, Japan
[2] NTT Communication Science Laboratories, 3-1 Morinosato Wakamiya, Atsugi, Kanagawa, Japan

E-mail: k-ishikawa@fuji.waseda.jp

Received 5 September 2020, revised 18 November 2020
Accepted for publication 27 November 2020
Published 11 February 2021

Abstract

Optical interferometric measurement methods for sound fields have garnered considerable attention owing to their contactless nature. The capabilities of non-invasive measurement and reconstruction of three-dimensional sound fields are significant for characterizing acoustic transducers. However, three-dimensional reconstructions are typically time consuming because of the two-dimensional scanning and rotation of the measurement system. This paper presents a scan and rotation-free reconstruction of an axisymmetric sound field in the human hearing range. A physical-model-based algorithm is proposed to reconstruct an axisymmetric sound field from optical interferograms recorded using parallel phase-shifting interferometry and a high-speed polarization camera. We demonstrate that audible sound fields can be reconstructed from data measured in 10 ms. The proposed method is effective for the rapid evaluation of axially symmetric acoustic transducers.

Keywords: optical sound measurement, parallel phase-shifting interferometry, high-speed camera, acousto-optic effect, Helmholtz equation, acoustic transducer

(Some figures may appear in colour only in the online journal)

1. Introduction

Acoustic transducers are key components for various acoustic applications; therefore, their measurement and evaluation are important in acoustics. For example, in acoustic metrology, the acoustic standard in air is realized using condenser microphones employed as a receiver and transmitter. In audio applications, loudspeaker units are ubiquitous in our daily lives for generating sounds in speech communication and music listening. Large-scale loudspeaker arrays have been used in spatial audio applications, such as sound field reproduction and acoustic virtual reality. Understanding sound radiations from individual transducers is essential for managing these applications accurately. Distant microphones are typically used for characterizing their spatial profiles, such as by directivity and acoustic intensity measurements. However, the measurement of three-dimensional (3D) sound fields to satisfy the spatial sampling theorem is difficult to achieve using microphones.

Optical methods are promising for measuring sound fields. Their contactless nature enables them to achieve

high-spatial-resolution measurements without contaminating the field to be measured, which is inevitable in conventional microphone measurements. The acousto-optic effect, i.e. light modulation caused by sound, enables acoustic information to be captured via optical measurement [1]. Such measurements are extensively used for various applications, e.g. imaging of sound fields generated by transducers [2–5], measurement of sound radiated by musical instruments [6–9], and calibration of microphones [10–12].

To obtain a 3D sound field from optical measurements, numerical reconstruction must be performed because the observed optical signals are proportional to the line integral of sound pressure. Computed tomography (CT) is the most typically used technique [1, 13–19], and a physical model-based algorithm has been proposed recently [20]. The reconstruction of a 3D sound field generally requires measurements of two-dimensional (2D) integrated fields from multiple angles, thereby necessitating the rotation of either measurement instruments or a sound field. This requirement significantly increases the measurement duration and complexity of the measurement system. However, rotation can be omitted when a sound field is axially symmetric because the line integral measurement is angle independent. A rotationally symmetric acoustic transducer operating in an axisymmetric mode typically exhibits an axially symmetric sound field. For high-intensity ultrasonic transducers, several methods have been proposed for scan- and rotation-free reconstructions, e.g. holographic interferometry [21], shadow graph [22, 23], and phase contrast [24, 25]. In these studies, underwater sound fields of magnitudes of the order of kilopascal to megapascal were reconstructed. However, such a reconstruction in the human hearing range, i.e. a sound pressure of less than 20 Pa and a frequency of less than 20 kHz, has not been achieved mainly because the optical modulation caused by audible sound is several orders of magnitude smaller than that caused by high-intensity ultrasound in water.

Herein, we propose a physical-model-based reconstruction method for an axially symmetric sound field from optical interferometric measurement, which can be applied to the sound in the human hearing range. The overview of the proposed method is depicted in figure 1. A sound field is optically captured using parallel phase-shifting interferometry (PPSI), which has recently been proposed for the high-speed imaging of sound fields [4, 26–29]. PPSI is suitable for the measurement of audible sound because of its frequency-independent high sensitivity. A high-speed camera can capture a sound field at a frame rate higher than the Nyquist frequency of the audible sound. Subsequently, an axisymmetric sound field is reconstructed from interferograms recorded via PPSI, as depicted in figure 1(b). We developed a reconstruction method based on the Helmholtz equation for an axisymmetric sound field. The sound fields radiated by a circularly symmetric loudspeaker were measured, and the reconstruction results were compared with the sound fields measured using a scanning microphone.

2. Measurement system

2.1. Acousto-optic effect

The principle underlying the interferometric observation of sound is known as the acousto-optic effect, which refers to the change in light properties when a light passes through a sound field [1]. The acousto-optic effect with a first-order approximation, which is acceptable for a weak sound field in air (pertaining to this study), can be derived using the Gladstone–Dale relation and adiabatic assumption:

$$n(\mathbf{r},t) = n_0 + \frac{n_0 - 1}{\gamma p_0} p(\mathbf{r},t), \tag{1}$$

where n is the refractive index modulated by sound pressure p; n_0 and p_0 are the refractive index and pressure under static conditions, respectively; and γ is the specific heat ratio. The geometric optics formulation describes the phase modulation of light propagating through a sound field as

$$\mathbf{E}(\mathbf{r},t) = \mathbf{E}_0(\mathbf{r},t)\mathrm{e}^{\mathrm{i}(\omega_\mathrm{l} t + \phi(\mathbf{r},t))}, \tag{2}$$

where $\mathbf{E}$ is the electric vector, $\mathbf{r} \in \mathbb{R}^3$ is the 3D position vector, t denotes time, $\mathbf{E}_0$ is the complex amplitude vector, $\mathrm{i} = \sqrt{-1}$, and ω_l is the angular frequency of light. The phase term ϕ is the product of the wavenumber of light and optical path length, i.e.

$$\begin{aligned} \phi(\mathbf{r},t) &= k_\mathrm{l} \int_{L(\mathbf{r})} n(\mathbf{l},t)\mathrm{d}\mathbf{l} \\ &= \phi_0(\mathbf{r}) + k_\mathrm{l} \frac{n_0 - 1}{\gamma p_0} \int_{L(\mathbf{r})} p(\mathbf{l},t)\mathrm{d}\mathbf{l}, \end{aligned} \tag{3}$$

where k_l is the wavenumber of light and $\phi_0 = k_\mathrm{l} n_0 |L(\mathbf{r})|$ denotes the static phase. Line integral is performed along the optical path $L(\mathbf{r})$, which can be assumed as a straight line because light bending caused by airborne sound is negligible. Equation (3) indicates that, by detecting the phase variation of the light passing through a sound field, the value proportional to the line integral of the sound pressure along the optical path can be obtained.

2.2. Optical instruments

To measure the phase variation of light caused by sound, we employed PPSI, which is a technique capable of single-shot observations of the optical phase by simultaneous detections of multiple phase-shifted interferograms [30, 31]; moreover, it has recently been applied to the high-speed imaging of sound fields [4, 26–29].

The schematics of the measurement system are shown in figure 2. The optical system is based on the Fizeau-type polarization interferometer [32]. The light source used was a Nd:YAG laser of wavelength 532 nm and of power 200 mW. The object light was transmitted through the optical flat, passed through the measurement area, reflected by the mirror,

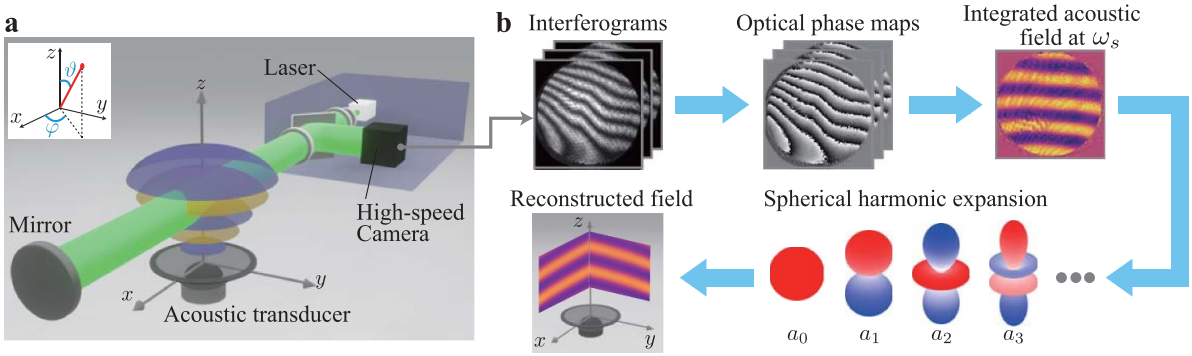

Figure 1. Overview of proposed method. (a) Sound field radiated by an axisymmetric acoustic transducer driven by sinusoidal wave at acoustic frequency ω_s, measured using PPSI. Blue and orange curved surfaces illustrate radiated sound waves. Light passing through the sound field is modulated by the sound. Modulated light interferes with reference light and interferograms that contain sound-field information, i.e. line integral of sound pressure along the laser path, is recorded using a high-speed camera. (b) 3D axisymmetric sound field reconstructed from recorded interferograms based on physical-model-based reconstruction method described in section 3. Optical phase maps are calculated from the interferograms, and integrated acoustic field at ω_s is extracted from phase maps. Subsequently, expansion coefficients of the solution to the spherical Helmholtz equation are numerically estimated. Finally, 3D sound field can be reconstructed by substituting the coefficients into the Helmholtz equation.

and transmitted through the optical flat again, whereas the reference light was reflected by the optical flat. The interfered light was detected by the high-speed polarization camera (PI-1P, Photron limited). The camera captured four phase-shifted interferograms simultaneously owing to a pixelated linear polarizer array mounted on an image sensor [33]. Subsequently, the optical phase difference between the object and reference light, $\Delta\phi$, was calculated from the four interferograms using the hyper ellipse fitting in a subspace (HEFS) method, whose performance is better than that of the ordinary four-step algorithm [34, 35].

The line integral of sound pressure was obtained from the optical phase map as follows. Because the difference between the object and reference paths is only the measurement area, $\Delta\phi$ is written as

$$\Delta\phi(y,z,t) = \Delta\phi_0 + 2k_l \frac{n_0 - 1}{\gamma p_0} \int_{x_1}^{x_2} p(\xi, y, z, t) \mathrm{d}\xi, \qquad (4)$$

where $\Delta\phi_0$ represents the static term, and the optical path is assumed to be parallel to the x-axis. The line integral of the sound pressure was obtained by dividing the measured phase by the environmental coefficient, $2k_l(n_0 - 1)/(\gamma p_0)$, and by removing the static component.

3. Reconstruction method

To reconstruct a sound field from a high-speed video of a 2D line integrated sound pressure field obtained by the measurement system, we present a physical-model-based approach using the Helmholtz equation. A reconstruction method based on the equation requiring multi-angle line integral measurements has been proposed previously, and the reconstruction errors are significantly fewer compared with those of the ordinal CT method [20]. In this study, to perform reconstruction from a single-angle measurement, we modeled the axisymmetric sound field using the Helmholtz equation in spherical coordinates. The reconstruction problem was formulated as the estimation of the expansion coefficients of the solution to the axisymmetric Helmholtz equation from the line integral values. The sound field can be reconstructed by substituting the estimated coefficients into the solution of the equation.

3.1. Physical model of axisymmetric sound field

Consider the Helmholtz equation in the spherical coordinates $(\zeta, \vartheta, \varphi)$ defined by $(x, y, z) = (\zeta\sin\vartheta\cos\varphi, \zeta\sin\vartheta\sin\varphi, \zeta\cos\vartheta)$ as depicted in the inset of figure 1(a). The Helmholtz equation for an acoustic frequency ω_s is written as

$$\left(\Delta_s + k_s^2\right) p(\zeta, \vartheta, \varphi, \omega_s) = 0, \qquad (5)$$

where

$$\Delta_s = \frac{1}{\zeta^2}\frac{\partial}{\partial\zeta}\left(\zeta^2\frac{\partial}{\partial\zeta}\right) + \frac{1}{\zeta^2\sin\vartheta}\frac{\partial}{\partial\vartheta}\left(\sin\vartheta\frac{\partial}{\partial\vartheta}\right) + \frac{1}{\zeta^2\sin^2\vartheta}\frac{\partial^2}{\partial\varphi^2}, \qquad (6)$$

and $k_s = \omega_s/c_s$ is the wavenumber of sound and c_s is the speed of sound. The solution to equation (5) can be expanded to

$$p(\zeta, \vartheta, \varphi, \omega_s) = \sum_{m=0}^{\infty}\sum_{m'=-m}^{m} a_{mm'} j_m(k_s\zeta) Y_m^{m'}(\vartheta, \varphi), \qquad (7)$$

where j_m is the mth order spherical Bessel function of the first kind,

$$Y_m^{m'}(\vartheta, \varphi) = \sqrt{\frac{2m+1}{4\pi}\frac{(m-m')!}{(m+m')!}} P_m^{m'}(\cos\vartheta)\, \mathrm{e}^{\mathrm{i}m'\varphi} \qquad (8)$$

is the spherical harmonic, $P_m^{m'}(x)$ is the associated Legendre polynomial, and $a_{mm'}$ is the coefficient [36].

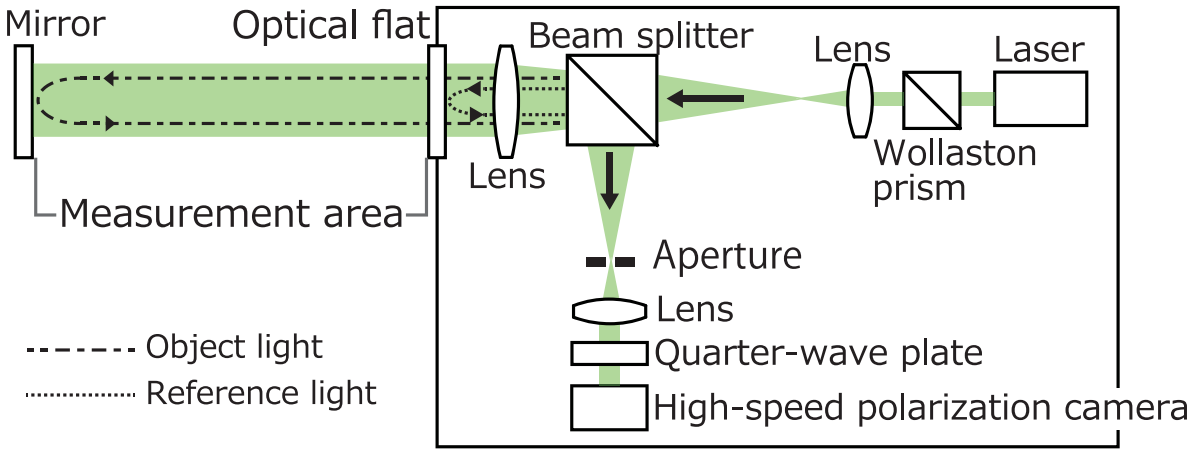

Figure 2. Schematics of optical system based on Fizeau-type polarization interferometer. Arrows indicate propagation directions of light. Line integral of sound pressure along object light within the measurement area is measured. High-speed polarization camera records the interferograms of the object and reference light.

As the sound fields in this study are axisymmetric, the solution can be modified to a simpler form. Using the z-axis as the symmetric axis, the sound field is independent of φ. Subsequently, the solution becomes

$$p(\zeta,\vartheta,\omega_s)=\sum_{m=0}^{\infty}a_m j_m(k_s\zeta)\sqrt{\frac{2m+1}{4\pi}}P_m(\cos\vartheta), \quad (9)$$

where $P_m(x)$ is the m-th order Legendre polynomial. Equation (9) indicates that any axisymmetric sound field can be determined by the set of expansion coefficients a_m.

3.2. Reconstruction from optical observation

To establish the reconstruction method in the frequency domain, a 2D complex integrated field at acoustic frequency ω_s is considered. The frequency domain representation of the data is written as

$$d_{\iota,\kappa}=\int_{x_1}^{x_2}p(\xi,y_\iota,z_\kappa,\omega_s)\mathrm{d}\xi, \quad (10)$$

where the pixel of the camera is specified by indices (ι,κ) and (y_ι,z_κ) is the position of the optical path corresponding to pixel (ι,κ). By substituting the solution of the Helmholtz equation into equation (10), the data can be written as

$$d_{\iota,\kappa}=\sum_{m=0}^{\infty}a_m\bar{\Upsilon}_{m,\iota,\kappa}, \quad (11)$$

where

$$\bar{\Upsilon}_{m,\iota,\kappa}=\int_{x_1}^{x_2} j_m(k_s\zeta(\xi,y_\iota,z_\kappa))\sqrt{\tfrac{2m+1}{4\pi}}P_m(\cos\vartheta(\xi,y_\iota,z_\kappa))\,\mathrm{d}\xi. \quad (12)$$

Herein, the integral term $\bar{\Upsilon}_{m,\iota,\kappa}$ is independent of the sound field to be reconstructed; it only depends on the measurement and reconstruction conditions such as the wavenumber of sound, optical path, and expansion order. For numerically estimating the expansion coefficients, the expansion order m is truncated by a finite number M. Therefore, equation (11) becomes

$$d_{\iota,\kappa}=\sum_{m=0}^{M}a_m\bar{\Upsilon}_{m,\iota,\kappa}. \quad (13)$$

This can be written in the matrix form as follows:

$$\mathbf{d}=\Upsilon\mathbf{a}, \quad (14)$$

where $\mathbf{d}$ is the data vector vectorized from matrix $(d_{\iota,\kappa})$, Υ is the matrix whose rows correspond to $\mathbf{d}$ and whose columns correspond to the expansion order, $\mathbf{a}=[a_1,\ldots,a_M]^{\mathrm{T}}$, and $^{\mathrm{T}}$ is the transpose.

The expansion coefficients $\mathbf{a}$ can be estimated by solving equation (14). For estimating coefficients $\mathbf{a}$, we employed a truncated singular value method as used previously [20]. The coefficient matrix Υ can be factorized by

$$\Upsilon=U\Sigma V^{\mathrm{H}}, \quad (15)$$

where U and V are unitary matrices, Σ is the diagonal matrix, and $^{\mathrm{H}}$ is the Hermitian transpose. The diagonal entries of Σ are set in the descending order as $\sigma_1\geqslant\sigma_2\geqslant\ldots$, where σ_i is the ith singular value. Therefore, the pseudo-inverse of Υ can be written by

$$\Upsilon^{\dagger}=V\Sigma^{\dagger}U^{\mathrm{H}}, \quad (16)$$

where $\Sigma^{\dagger}=\mathrm{diag}(1/\sigma_1,1/\sigma_2,\ldots)$, and $\mathrm{diag}(\cdot)$ denotes the function constructs of a square diagonal matrix. Because large components of $\Sigma^{\dagger}$ are affected significantly by measurement noise, the reconstruction becomes unstable. To reduce this effect, the singular values were truncated by a threshold τ as follows:

$$\Sigma_{\tau}^{\dagger}=\mathrm{diag}(1/\sigma_1,1/\sigma_2,\ldots,0,\ldots,0), \quad (17)$$

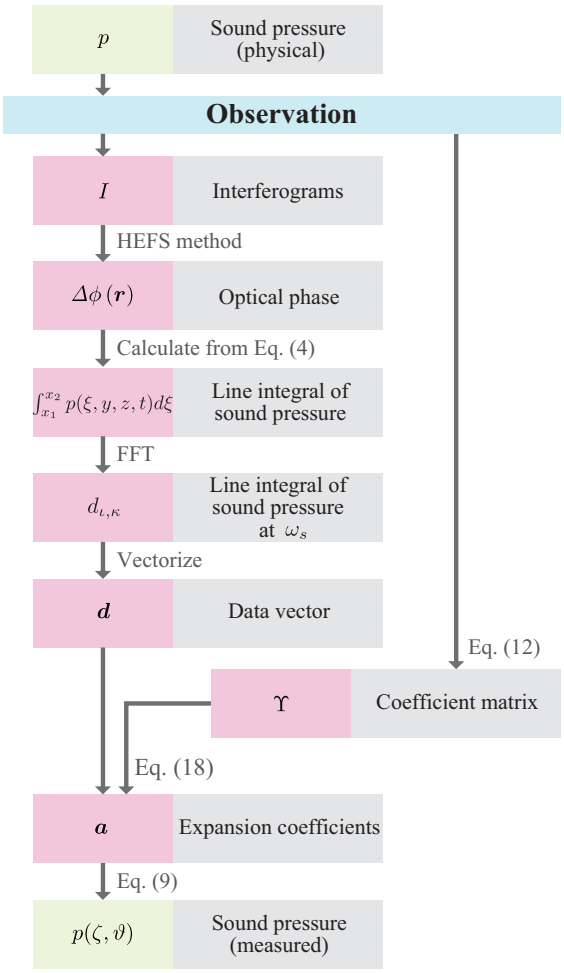

Figure 3. Calculation procedure of proposed method.

where all diagonal entries of $\Sigma^\dagger$ satisfying $\sigma_i < \tau\sigma_1$ were replaced by zero. Finally, the coefficient vector $\mathbf{a}$ can be calculated by

$$\mathbf{a} = \Upsilon_\tau^\dagger \mathbf{d} = V\Sigma_\tau^\dagger U^{\mathrm{H}}\mathbf{d}. \tag{18}$$

Once $\mathbf{a}$ is estimated, the sound pressure values at arbitrary positions can be reconstructed by substituting $\mathbf{a}$ into equation (9).

3.3. Calculation procedure

Next, we summarize the reconstruction procedure. The flowchart is illustrated in figure 3. An axisymmetric sound field at acoustic frequency ω_s was observed using the optical system described in section 2.2. Each image recorded by the high-speed polarization camera comprised four phase-shifted interferograms, from which optical phase values were calculated using the HEFS method [34, 35]. Subsequently, one-dimensional unwrapping was performed along the temporal direction. The line integrals of sound pressure can be obtained by dividing the unwrapped phase by the environmental constant $2k_1(n_0 - 1)/(\gamma p_0)$. Subsequently, the matrix representing the integrated sound field at ω_s was obtained by calculating the time-directional Fourier transform to each pixel and extracting the frequency component at ω_s. Finally, the data vector $\mathbf{d}$ was obtained by vectorizing the matrix.

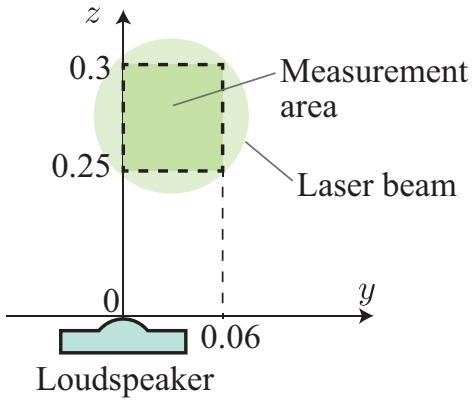

Figure 4. Cross-sectional view of experimental configuration.

Table 1. Experimental conditions.

Optical system	
Integral path	$-1.25 \leqslant x \leqslant 1.25$
Measurement area	60 mm × 50 mm
Image resolution	(87, 72)
Frame rate	50 kfps
Camera shutter	20 μs
Number of images	500
Laser wavelength	532 nm
Laser power	200 mW
Reconstruction	
Expansion order M	5
Truncation threshold τ	10^{-3}
Microphone scanning	
Microphone	1/4 inch (BK 4939)
Scanning area	60 mm × 50 mm
Scanning step	5 mm
Sampling frequency	50 kHz

The coefficient matrix Υ was calculated from the measurement and reconstruction conditions using equation (12). To calculate the matrix elements, the coordinate must be determined. Although the origin can be at an arbitrary position along the symmetric axis, its position affects the expansion coefficients. To efficiently represent an original sound field with a small expansion order, the origin of the coordinate should be at the acoustic center of the sound source. Calculating equation (12) for every pixel and every order yields Υ.

Once $\mathbf{d}$ and Υ were obtained, the coefficient vector $\mathbf{a}$ was estimated using the truncated singular value decomposition (TSVD). Finally, by substituting $\mathbf{a}$ in equation (9), the original sound field was reconstructed.

Two arbitrary parameters were used for the reconstruction: the expansion order of the solution of the Helmholtz equation M and the threshold of TSVD τ. A greater M provides a better representation of a complicated sound field; however, the overfitting risk and computational time increase. The threshold

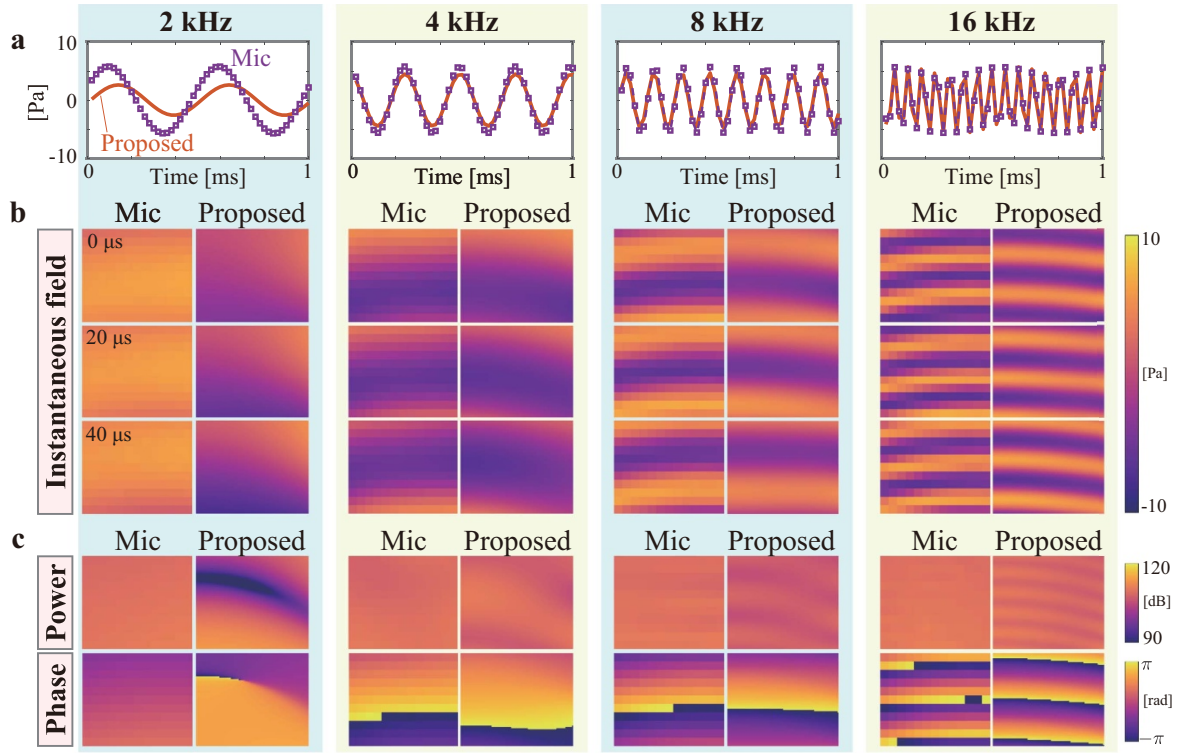

Figure 5. Experimental results. (a) Temporal waveforms extracted from reconstructed field and measured using microphone at $(x, y, z) = (0, 0, 0.3)$. (b) Instantaneous pressure fields measured using scanning microphone and obtained by the proposed method. (c) Power and phase maps at acoustic frequencies. Microphone results of (b) and (c) are horizontally flipped for ease of comparison.

τ determines the number of singular values used for estimating the coefficient vector of the solution. When τ is extremely large, the reconstructed sound field cannot represent the original field; meanwhile, the measurement noise violates the reconstructed results when τ is extremely small. These parameters should be determined based on the measured data and conditions.

4. Experiments

4.1. Setup

A proof-of-concept experiment verifying the feasibility of the proposed method was conducted. The sound fields reconstructed using the proposed method were compared with those measured using scanning a quarter-inch microphone. A rotationally symmetric loudspeaker (FOSTEX FT48D) was used as the axisymmetric sound source. The input signals of the loudspeaker were sinusoidal waves of frequencies 2, 4, 8, and 16 kHz. We confirmed that the angular deviations of the radiated sound pressure level were less than 1 dB for those frequencies. Sound absorption materials were used to cover the walls, ceiling, and floor of the experimental room to reducing reflected sounds, which may hinder the axisymmetry of the sound field.

The cross-sectional view of the experimental configuration is illustrated in figure 4, and the details of the measurement conditions are listed in table 1. The center of the diaphragm was defined as the origin of the coordinate. Because the sound fields were symmetric with respect to the z-axis, only the positive region of the y-axis was used. A rectangular area measuring 60 mm $\times$ 50 mm within the laser beam was used as data for the reconstruction, as depicted by the dashed lines. The image resolution of the rectangular area was 87 $\times$ 72, indicating that the interval between adjacent pixels was 0.7 mm. A quarter-inch free-field microphone was scanned over the same area at the $x = 0$ plane with a scanning step of 5 mm using a 2D traverse unit. The reconstruction parameters, $M = 5$ and $\tau = 10^{-3}$, were determined manually. The reconstruction area was the same that from the microphone measurement: $(0, 0, 0.25) \leqslant (x, y, z) \leqslant (0, 0.06, 0.3)$. The acquisition timings of the camera and microphone signal were aligned with respect to the input sinusoidal wave, whereas their sampling clocks were not synchronized. The high-speed camera captured 500 images with a frame rate of 50 000; the measurement duration of the PPSI was 10 ms. The microphone scanning required approximately 10 min.

The environmental factors in the measurement room were as follows. The temperature, humidity, and static pressure were 23.4 °C, 33.7%, and 100 010 Pa, respectively. The speed of sound, c_s, was 345.6 m s^{-1}. The static refractive index, n_0, was calculated as 1.000 266 using Ciddor's equations [37]. The specific heat ratio, γ, was 1.40. Therefore, the environmental coefficient, $2k_l\,(n_0 - 1)\,/\,(\gamma p_0)$, was 0.045 rad/Pa.

4.2. Results

Figure 5 shows the experimental results. The reconstructed waveforms at $(x, y, z) = (0, 0, 0.3)$ plotted in figure 5(a) agree

well with the waveforms measured using the microphone at the same position except for 2 kHz. The measured and reconstructed instantaneous sound fields are shown in figure 5(b). The intervals of the depicted images are 20 μs, within which sound propagates approximately 6.9 mm. The spatiotemporal profiles of both fields are consistent for 4, 8, and 16 kHz. These results confirmed the validity of the proposed method for those frequencies.

The power and phase maps of the measured and reconstructed fields are shown in figure 5(c). Owing to the low spatial resolution of the microphone scanning, the phase maps obtained from the microphone measurements are not smooth, whereas the proposed method is able to reconstruct the smooth curvatures of the phase discontinuities. As shown in figure 5(c), the reconstructed power maps exhibit periodic patterns correlated to their instantaneous fields. The period of the power fluctuation is half the acoustic wavelength. Such periodic fluctuations may appear when the propagating sound wave and non-propagating vibration are superimposed at the same frequency. The non-propagating vibration at the acoustic frequency can imply a pseudo signal that is associated with the mechanical vibration of optical components caused by the sound wave incident on them. The pseudo signal is an inevitable side effect of the optical sound measurement because it is caused by the sound to be measured. For our experiments, the pseudo signal imposed a limited effect on the visualization of the instantaneous fields; however, it should be addressed when absolute pressure values are important. Tightly fixing optical components and physically separating the acoustic field and optical instruments should reduce this effect. In addition, the pseudo signal may be eliminated by a spatiotemporal filtering method that extracts signals satisfying the Helmholtz equation from noisy data because the pseudo signal does not obey the Helmholtz equation [5, 38, 39].

5. Discussions and conclusions

The infeasibility of the reconstruction of the 2 kHz sound field was due to its long wavelength. As indicated by the field measured using the microphone, the 2 kHz sound wave was almost in-phase within the measurement area. This means that the acoustic phase differences between adjacent pixels were small; the reconstruction might suffer significantly by small measurement noise. The ratios of the acoustic wavelengths ($\lambda_s = 2\pi c_s/\omega_s$) to the length of the measurement area along the z-axis (0.05 m) were 0.29, 0.58, 1.16, and 2.31 for 2, 4, 8, and 16 kHz, respectively. For 2 kHz, only less than one-third of the acoustic wavelength was captured by each image. The reconstructed field of 4 kHz indicated a small discrepancy, as shown in the phase map (bottom of figure 5(c)), where each image comprised approximately a half period of the sound wave. These results suggest that the lowest frequency limit depends on the ratio between the acoustic wavelength and measurement area. Therefore, to apply this method for lower frequencies, the measurement area must be expanded. The highest frequency is currently limited by the frame rate of the camera.

In summary, the proof-of-concept experiment confirmed that the sound fields radiated by the circularly symmetric loudspeaker with a sound pressure of approximately 5 Pa and frequencies of 4, 8, and 16 kHz were successively reconstructed; this is the first demonstration of the scan and rotation-free reconstruction of 3D sound fields in the human hearing range. Because each measurement required only 10 ms, the proposed method will be highly beneficial when a rapid evaluation is important, such as in transducer design, fabrication processes, and testing of individual transducers for large-scale array systems. Future studies should include the optimization of the estimation parameters and expansion of the frequency limits.

Acknowledgment

This work is partly supported by Japan Society for the Promotion of Science (JSPS) Grant-in-Aid for JSPS Research Fellow (16J06772).

ORCID iDs

Kenji Ishikawa https://orcid.org/0000-0003-0423-566X
Kohei Yatabe https://orcid.org/0000-0002-1345-0663

References

[1] Torras-Rosell A, Barrera-Figueroa S and Jacobsen F 2012 Sound field reconstruction using acousto-optic tomography *J. Acoust. Soc. Am.* **131** 3786–93
[2] Zipser L and Lindner S 2001 Visualisation of vortexes and acoustic sound waves *Proc. 17th Int. Congr. Acoust.* pp 144–7
[3] Bertling K, Perchoux J, Taimre T, Malkin R, Daniel Robert A D and Bosch T 2014 Imaging of acoustic fields using optical feedback interferometry *Opt. Express* **22** 30346–56
[4] Ishikawa K, Yatabe K, Chitanont N, Ikeda Y, Oikawa Y, Onuma T, Niwa H and Yoshii M 2016 High-speed imaging of sound using parallel phase-shifting interferometry *Opt. Express* **24** 12922–32
[5] Chitanont N, Yatabe K, Ishikawa K and Oikawa Y 2017 Spatio-temporal filter bank for visualizing audible sound field by Schlieren method *Appl. Acoust.* **115** 109–20
[6] Pandya B H, Settles G S and Miller J D 2003 Schlieren imaging of shock waves from a trumpet *J. Acoust. Soc. Am.* **114** 3363–7
[7] Gren P, Tatar K, Granström J, Molin N-E and Jansson E V 2006 Laser vibrometry measurements of vibration and sound fields of a bowed violin *Meas. Sci. Tech.* **17** 635–44
[8] Olsson E and Tatar K 2006 Sound field determination and projection effects using laser vibrometry *Meas. Sci. Tech.* **17** 2843–51
[9] Rendón P L, Velasco-Segura R, Echeverría C, Porta D, Pérez-López A, Vázquez-Turner R T and Stern C 2018 Using Schlieren imaging to estimate the geometry of a shock wave radiated by a trumpet bell *J. Acoust. Soc. Am.* **144** EL310–4
[10] Yuldashev P, Karzova M, Khokhlova V, Ollivier S and Blanc-Benon P 2015 Mach-Zehnder interferometry method for acoustic shock wave measurements in air and

broadband calibration of microphones *J. Acoust. Soc. Am.* **137** 3314–24
[11] Torras-rosell A and Barrera-figueroa S 2015 An acousto-optic method for free-field microphone calibration *Proc. Int. Congr. Sound Vib.* pp 12–16
[12] Zheng X, Chen H, Yan X, Qian M and Cheng Q 2017 Quantitative calibration of sound pressure in ultrasonic standing waves using the Schlieren method *Opt. Express* **25** 20401–9
[13] Lokberg O J, Espeland M and Pedersen H M 1995 Tomographic reconstruction of sound fields using TV holography *Appl. Opt.* **34** 1640–5
[14] Pitts T A, Sagers A and Greenleaf J F 2001 Optical phase contrast measurement of ultrasonic fields *IEEE Trans. Ultrason. Ferroelectr. Freq. Control* **48** 1686–94
[15] Oikawa Y, Ikeda Y, Goto M, Takizawa T and Yamasaki Y 2005 Sound field measurements based on reconstruction from laser projections *Proc. IEEE Int. Conf. Acoust., Speech, Signal Process.* pp 661–4
[16] Sakoda T and Sonoda Y 2008 Visualization of sound field with uniform phase distribution using laser beam microphone coupled with computerized tomography method *Acoust. Sci. Tech.* **29** 295–9
[17] Bahr L and Lerch R 2008 Sound pressure measurement utilizing light refractive tomography *Proc. IEEE Ultrason. Symp.* 840–3
[18] Ikeda Y, Okamoto N, Konishi T, Oikawa Y, Tokita Y and Yamasaki Y 2016 Observation of traveling wave with laser tomography *Acoust. Sci. Tech.* **37** 231–8
[19] Koponen E, Leskinen J, Tarvainen T and Pulkkinen A 2019 Acoustic pressure field estimation methods for synthetic schlieren tomography *J. Acoust. Soc. Am.* **145** 2470–9
[20] Yatabe K, Ishikawa K and Oikawa Y 2017 Acousto-optic back-projection: physical-model-based sound field reconstruction from optical projections *J. Sound Vib.* **394** 171–84
[21] Hisada S, Suzuki T, Nakahara S and Fujita T 2002 Visualization and measurements of sound pressure distribution of ultrasonic wave by stroboscopic real-time holographic interferometry *Japan. J. Appl. Phys.* **41** 3316–24
[22] Omura R, Shimazaki Y, Yoshizawa S and Umemura S 2011 Quantitative measurement of focused ultrasound pressure field using subtraction shadowgraph *Japan. J. Appl. Phys.* **50** 4–7
[23] Miyasaka R, Yasuda J, Syahid M, Yoshizawa S and Umemura S I 2014 Quantitative measurement of focused ultrasound pressure field by background-subtracted shadowgraph using holographic diffuser as screen *Japan. J. Appl. Phys.* **53** 07KF24
[24] Harigane S, Miyasaka R, Yoshizawa S and Umemura S 2013 Optical phase contrast mapping of highly focused ultrasonic fields *Japan. J. Appl. Phys.* **52** 07HF07
[25] Oyama S, Yasuda J, Hanayama H, Yoshizawa S and Umemura S 2016 Quantitative measurement of ultrasound pressure field by optical phase contrast method and acoustic holography *Japan. J. Appl. Phys.* **55** 07KB09
[26] Ishikawa K, Tanigawa R, Yatabe K, Oikawa Y, Onuma T and Niwa H 2018 Simultaneous imaging of flow and sound using high-speed parallel phase-shifting interferometry *Opt. Lett.* **43** 991–4
[27] Tanigawa R, Ishikawa K, Yatabe K, Oikawa Y, Onuma T and Niwa H 2018 Optical visualization of a fluid flow via the temperature controlling method *Opt. Lett.* **43** 3273–6
[28] Yatabe K, Tanigawa R, Ishikawa K and Oikawa Y 2018 Time-directional filtering of wrapped phase for observing transient phenomena with parallel phase-shifting interferometry *Opt. Express* **26** 13705–20
[29] Hermawanto D, Ishikawa K, Yatabe K and Oikawa Y 2020 Determination of frequency response of MEMS microphone from sound field measurements using optical phase-shifting interferometry method *Appl. Acoust.* **170** 107523
[30] Awatsuji Y, Sasada M and Kubota T 2004 Parallel quasi-phase-shifting digital holography *Appl. Phys. Lett.* **85** 1069–71
[31] Millerd J E, Brock N J, Hayes J B, North-Morris M B, Novak M and Wyant J C 2004 Pixelated phase-mask dynamic interferometer *Proc. SPIE* **5531** 304–14
[32] Yatagai T *et al* 2015 Instantaneous phase-shifting Fizeau interferometry with high-speed pixelated phase-mask camera *SPECKLE 2015* **9660** 237–40
[33] Onuma T and Otani Y 2014 A development of two-dimensional birefringence distribution measurement system with a sampling rate of 1.3 MHz *Opt. Commun.* **315** 69–73
[34] Yatabe K, Ishikawa K and Oikawa Y 2017 Simple, flexible and accurate phase retrieval method for generalized phase-shifting interferometry *J. Opt. Soc. Am.* A **34** 87–96
[35] Yatabe K, Ishikawa K and Oikawa Y 2017 Hyper ellipse fitting in subspace method for phase-shifting interferometry: practical implementation with automatic pixel selection *Opt. Express* **25** 29401–16
[36] Williams E G 1999 Spherical waves *Fourier Acoustics* ed E G Williams (London: Academic) pp 183–234
[37] Ciddor P E 1996 Refractive index of air: new equations for the visible and near infrared *Appl. Opt.* **35** 1566–73
[38] Tanigawa R, Yatabe K and Oikawa Y 2019 Guided-spatio-temporal filtering for extracting sound from optically measured images containing occluding objects *Proc. IEEE Int. Conf. Acoust., Speech, Signal Process.* pp 945–9
[39] Chitanont N, Thongtangsai P, Tachatanachai D, Chatsuksiridech P, Imaeda F, Tanigawa R, Yatabe K and Oikawa Y 2020 Noise reduction by spatio-temporal filtering on parallel phase-shifting interferometry *6th Int. Conf. Eng. Appl. Sci. Tech. (ICEAST)* pp 1–4